Ultralow-loading Pt/Zn hybrid cluster in zeolite HZSM-5 for efficient dehydroaromatization

Genwei Chen,[1] Lingzhe Fang,[2] Tao Li,[2,3] Yizhi Xiang[1*]

1. Dave C. Swalm School of Chemical Engineering, Mississippi State University, MS State, MS 39762, United States

2. Department of Chemistry and Biochemistry, Northern Illinois University, DeKalb, Illinois 60115, United States

3. X-ray Science Division, Argonne National Laboratory, Lemont, Illinois 60439, United States

Abstract: Minimizing Pt loading without sacrificing catalytic performance is critical, particularly for designing cost-efficient hydrocarbon transformation catalysts. Here, we show that ultralow-loading (0.001-0.05 wt%) Pt and Zn functionalized HZSM-5 catalysts, prepared through simple ion-exchange and impregnation, is highly active and stable for light alkanes dehydroaromatization (DHA). The specific activity of BTX is up to 8.2 mol/g_{Pt}/min (or 1592 min^{-1}) over the 0.001 wt% Pt-Zn_2/HZSM-5 catalyst during ethane DHA at 550ºC under atmospheric pressure. Additionally, such bimetallic Pt_x-Zn_y/HZSM-5 catalysts are highly stable in contrast to the monometallic Pt/HZSM-5 catalysts. The rate constant of deactivation ($k_{deactiv}$), according to the first-order generalized power-law equation model, for the bimetallic catalysts is up to 120 times lower than the monometallic counterparts depending on the Pt loading. This breakthrough is achieved owing to the formation of $[Pt_1\text{-}Zn_n]^{\delta+}$ hybrid cluster, instead of Pt^0 clusters-proton adducts, in the micropores of ZSM-5 zeolite.

Keywords: Light alkanes, dehydroaromatization, Pt/Zn clusters, HZSM-5

Introduction

The production of BTX (benzene, toluene, and xylene) and light olefins – both are critical building blocks of the chemical industry – currently rely heavily on steam cracking with naphtha (from the petroleum) as the feedstock. Such a process is carbon- and energy-intensive as it requires a high reaction temperature of up to 900 ºC due to the absence of a catalyst. Therefore, the "on-purpose" production of BTX and light olefins selectively from the cheaper and abundant light alkanes (from the shale gas) through the catalytic dehydroaromatization (DHA) and dehydrogenation (DH) could be very important complements for the noncatalytic steam cracking process.

The transformation of light alkanes through DHA/DH has been extensively studied recently due to the urgent need for upgrading the low-cost natural gas liquids (NGLs).[1-11] The production of NGLs in the US is up to 5.91 million barrels/day, among which more than 90% is ethane and propane.[12] While the DHA of propane has been demonstrated in the industry by UOP/BP (known as Cyclar™ process) using Ga/HZSM-5 as the catalyst,[13] the state-of-the-art DHA catalyst still faces challenges of insufficient activity and stability for ethane DHA. Based on the catalytic pathways,[14] an efficient DHA catalyst should show balanced activities for dehydrogenation, oligomerization, and cyclization, respectively, which requires optimized metal/acid functionalities. Specifically, the metal sites in/on zeolites, such as $metal^0$/metal oxide clusters, $metal^{\delta+}$ cations (Lewis acids), and metal carbides or oxycarbides, are critical to the initial C-H bond activation,[4, 15] and could facilitate the release of H_2 through hydrogen

back-spillover.[16-18] Whereas, the Brønsted acid sites of the zeolite are essential for oligomerization and cyclization,[5, 19] and the MFI zeolite with 3D micropore framework structure is preferred to suppress the formation of polycondensed aromatic molecules (the pore diameters of MFI zeolite are similar to the kinetic diameters of BTX molecules: ~ 6Å).[4]

The different metals, such as Pt,[20-21] Zn,[22-23] Ga,[24-25] and Mo,[26-27] modified HZSM-5 catalysts have been widely studied in ethane DHA. The Pt/HZSM-5 catalysts have been frequently patented[28-32] due to the higher activity. The Pt^0 nanoparticle and the electron deficiency $[Pt_m\text{-}H_n]^{n+}$ metal-proton adducts (in zeolite) have a high affinity with the paraffinic C-H bond,[33-34] which renders its exceptional performance in the hydrocarbons conversions. However, the high cost and scarcity of Pt strongly restricted the application of the Pt/HZSM-5 catalyst: most of the recent works employ up to 0.1-1 wt% of Pt in their DHA catalysts,[9, 35-36] which are 100-1000 time more expensive than the Cyclar catalyst. To the best of our knowledge, Pt loading as low as 0.04 wt% was only reported in previous Shell patents,[28-30] and it remains a formidable challenge to design an efficient DHA catalyst with ultralow-loading (≤0.01 wt%) Pt. As the Pt loading decreases, the dispersion and the electron deficiency of the Pt species will increase due to the formation of $[Pt_m\text{-}H_n]^{n+}$ metal-proton adducts, which could stabilize the platinum-ethylene complex and lead to the formation of heavier oligomers (coke precursor) due to the scaling relationship.[37] Therefore, decreasing the Pt loading will not only decrease the activity but also stability due to the increased rate of coke deposition.

According to the literature, the second metal promoter could modify the surface electronic structure/state of Pt, which will influence the availability and energies of the valence electrons to form chemical bonds with adsorbates.[38] Miller and Greeley suggested that Zn modified the energy of the Pt 5d electrons, which directly relates to the enhanced activity and selectivity during ethane dehydrogenation.[34] Here we show that the activity and stability of the ultralow-loading (0.001-0.01 wt%) Pt/HZSM-5 catalyst in ethane DHA can be significantly increased through "hybridizing" Pt with Zn (II) cations inside the micropore of HZSM-5. Such "Pt/Zn hybrid clusters" in HZSM-5 zeolite are different from the intermetallic or single atom alloys reported in the literature since the majority of the Zn species in the HZSM-5 remain as Zn (II) cation Lewis acids. Because the proton (H^+) was exchanged by the Zn (II) cation, the highly dispersed Pt in such catalyst could "hybridize" with the Zn (II), forming $[Pt_1\text{-}Zn_n]^{\delta+}$ cluster, which shows weaker Pt-ethylene interaction than the electron deficiency $[Pt_m\text{-}H_n]^{n+}$ metal-proton adducts in the monometallic Pt/HZSM-5 catalyst.

Results and discussion

Catalyst activity and deactivation: The catalysts consisting of $[Pt_1\text{-}Zn_n]^{\delta+}$ hybrid clusters were prepared through ion exchange of Zn (II) cation followed by wet-impregnation of Pt. The obtained samples were activated in 10% H_2 at 650 ºC to facilitate the formation of $[Pt_1\text{-}Zn_n]^{\delta+}$ adducts. The Zn loading in HZSM-5 was adjusted by the time of ion exchange. The catalysts were designated as $Pt_x\text{-}Zn_y$/HZSM-5 (or simply Pt_xZn_y), where *x* wt% is the nominal loading of Pt and *y* wt% is the Zn loading according to ICP-MS. The catalytic performance of the bimetallic $Pt_x\text{-}Zn_y$/HZSM-5 and the corresponding monometallic catalysts during ethane DHA will be mainly discussed based on the space-time yield (STY) of BTX and ethylene, ethane conversion, and BTX selectivity as a function of time on stream (TOS). The influence of Zn and Pt loading on the activity, selectivity, and stability are shown in Fig. 1. Further catalytic data can be found in Table S1 and Fig. S1-S4.

The most intriguing observation from the catalytic data is the high stability of the bimetallic Pt_x-Zn_y/HZSM-5 catalysts with ultralow Pt loading (0.001-0.05 wt%). Noteworthily, the monometallic Pt/HZSM-5 catalysts with such ultralow Pt loading are not efficient for ethane DHA. As shown in Fig. S1, although the monometallic ultralow loading Pt/HZSM-5 catalysts are also active for ethane DHA, the activity, selectivity, and especially stability decrease significantly with decreasing Pt loading. For example, the monometallic $Pt_{0.005}$/HZSM-5 catalyst shows an initial STY of BTX and ethylene of 45 and 180 μmol/g/min (Fig. S1 b-c), respectively, and the catalyst totally deactivated after TOS only around 1 h. The corresponding initial ethane conversion is 7% (Fig. S1a) and the initial BTX selectivity is only 26% (Fig. S1d). With the increase of Pt loading to 0.01 wt%, the initial STY of BTX and ethylene increased to 150 and 280 μmol/g/min, respectively, and the lifespan of the catalyst increased to 4 h. The activity and durability further increased with increasing Pt loading to 0.05 wt% (the lowest Pt loading reported in the literature for ethane DHA), however, the catalyst was still totally deactivated within 16 h TOS. The lower activity and short durability are most likely the reason for the absence of literature on the DHA with ultralow loading Pt-based catalysts.

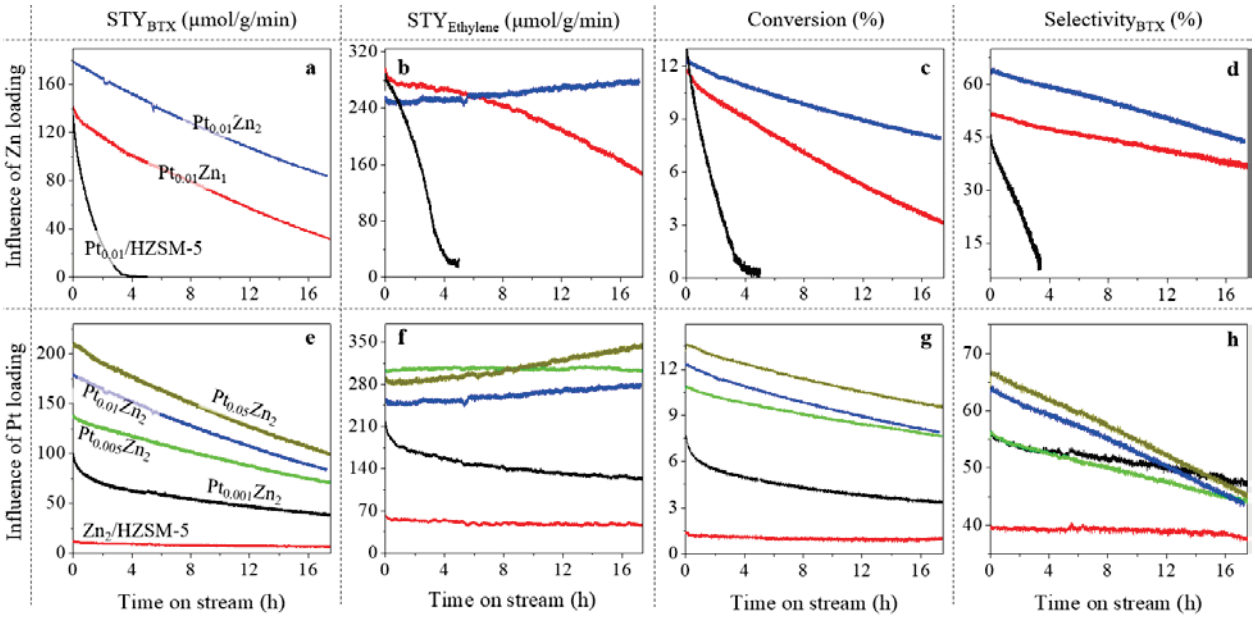

Fig. 1 Catalytic data in terms of STY of BTX and ethylene, conversion, and BTX selectivity during ethane DHA. (a-d) influence of Zn loading, (e-h) influence of Pt loading. The reactions were performed over 100 mg of catalyst at 550ºC under atmospheric pressure of pure ethane (20 mL/min), GHSV≈6000 h^{-1}.

In contrast to the monometallic Pt/HZSM-5, the bimetallic Pt_x-Zn_y/HZSM-5 catalysts demonstrated significantly higher stability and BTX selectivity. Fig. 1 (a-d) shows the influence of Zn loading (keeping the Pt loading constant at 0.01 wt%) on the activity, selectivity, and stability. It is seen that, over the $Pt_{0.01}$-Zn_2/HZSM-5 catalyst, the initial STY of BTX is up to 175 μmol/g/min (1.75 mol/g_{Pt}/min or 341 min^{-1}) and it remains > 50% of the initial STY after 17 h TOS. It takes > 65 h for the total deactivation towards the formation of BTX (see Fig. S2), which is more than 18 times longer than the monometallic $Pt_{0.01}$/HZSM-5. Meanwhile, the initial STY of ethylene is 240 μmol/g/min, which even increases slightly with TOS and reaches the maximum after 25-30 h then slightly decreased. No significant deactivation towards ethylene formation was observed even up to 65 h TOS (see Fig. S2).

The corresponding initial ethane conversion is 12% and the initial BTX selectivity is 63%. Additionally, the selectivity of CH_4 and C_3-C_5 hydrocarbons is only 10% (see Figs. S3-S4).

The influence of Pt loading (varied between 0.001 and 0.05 wt%) on the catalytic performance was evaluated at a constant Zn loading of 2 wt%. As shown in Fig. 1 (e-h), without Pt, the monometallic Zn_2/HZSM-5 catalyst shows very low activity for ethane DHA under the investigated conditions. Ethane conversion is below 1.3% and the initial STY of BTX is only 12 μmol/g/min. Nonetheless, with the presence of ultralow amounts of Pt (0.001 wt%), the STY of BTX and ethylene, ethane conversion, and BTX selectivity all increased significantly. The initial STY of BTX is up to 100 μmol/g/min, more than 8 times the Zn_2/HZSM-5. The activity of the catalysts further increased with increasing the Pt loading from 0.001 to 0.05 wt%. However, the specific activity per gram of Pt (see Fig. S5) significantly decreased with increasing Pt loading. Noteworthily, the STY of ethylene slightly decreased with TOS for the $Pt_{0.001}Zn_2$/HZSM-5 (Fig. 1f), but it is more stable and even slightly increased for the catalysts with a higher Pt loading. To the best of our knowledge, the present Pt-Zn/HZSM-5 is the most active and stable catalyst for ethane DHA for BTX and ethylene (see Table S1), especially considering that the Pt loading in our catalyst is 50-1000 times lower than that reported in the literature.

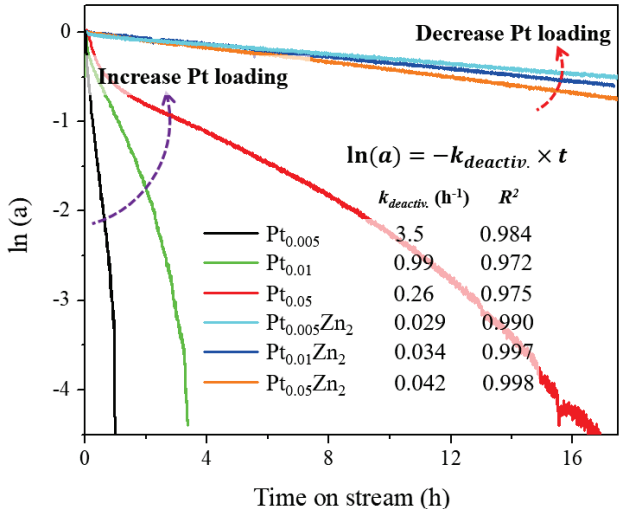

Fig. 2 Deactivation kinetics of BTX during ethane DHA over the Pt_x-Zn_2/HZSM-5 and Pt_x/HZSM-5 catalysts at 550ºC. The deactivation rate constants ($k_{deactiv}$) were calculated based on the first order GPLE model by fitting the linear relationships between ln (a) and time ($\ln(a) = -k_{deactiv.} \times t$, where "$a$" is the reactivity coefficient).

As we have already seen, the bimetallic Pt_x-Zn_2/HZSM-5 catalysts demonstrated outstanding stability during ethane DHA, although their monometallic Pt_x/HZSM-5 counterparts deactivate extremely fast due to the ultralow Pt loading. Further information about the stability can be found from the deactivation kinetics analysis based on the generalized power-law equation (GPLE) model.[39-40] As shown in Fig. 2, the deactivation of BTX on the bimetallic Pt_x-Zn_2/HZSM-5 catalysts follows strictly the first order GPLE model ($\ln(a) = -k_{deactiv.} \times t$, where "$a$" is the reactivity coefficient). The deactivation rate constant ($k_{deactiv}$) is only 0.029 h^{-1} for the $Pt_{0.005}$-Zn_2/HZSM-5, although the $k_{deactiv}$ slightly increased to 0.034 and 0.042 h^{-1} with increasing Pt loading to 0.01 and 0.05 wt%, respectively. Unlike the bimetallic catalysts, which show decreased deactivation with decreasing Pt loading, the

monometallic Pt_x/HZSM-5 catalysts show decreased deactivation with increasing Pt loading. The $k_{deactiv}$ for the monometallic Pt_x/HZSM-5 obtained by fitting the first order GPLE model is 3.5, 0.99, and 0.26 h^{-1} for the catalysts with Pt loading of 0.005, 0.01, 0.05 wt%, respectively, although the deactivation kinetics deviate significantly from the first order (and the second-order) GPLE models. We suggested that different deactivation mechanisms might be involved in the monometallic Pt_x/HZSM-5. Noteworthily, the $k_{deactiv}$ of the $Pt_{0.005}$-Zn_2/HZSM-5 is very similar to the Zn_2/HZSM-5 (see Fig. S6), and it is 120 times lower than the monometallic $Pt_{0.005}$/HZSM-5.

While the present Pt_x-Zn_y/HZSM-5 catalyst demonstrated outstanding activity and stability, it must be admitted that the regenerability of the present catalyst needs to be further optimized. As shown in Fig. S7, the initial ethane conversion decreased by about 10% after regeneration in 20% O_2 at 550 ºC for 2 h. Nonetheless, the regenerability of the bimetallic catalyst is improved in contrast to the monometallic $Pt_{0.01}$/HZSM-5 counterpart (the latter deactivates significantly faster after regeneration), indicating that the presence of Zn enhanced the stability of the Pt species. We advocate that the high mobility of both Pt and Zn species be responsible for the irreversible deactivation during the reaction and regeneration. Noteworthily, zinc evaporation has been identified as the key reason for the irreversible catalyst deactivation during dehydrogenation.[41] Additionally, the structural transformation of the Pt species in zeolite under both reductive and oxidative conditions has been identified by the Corma group and his collaborators at ExxonMobil.[42]

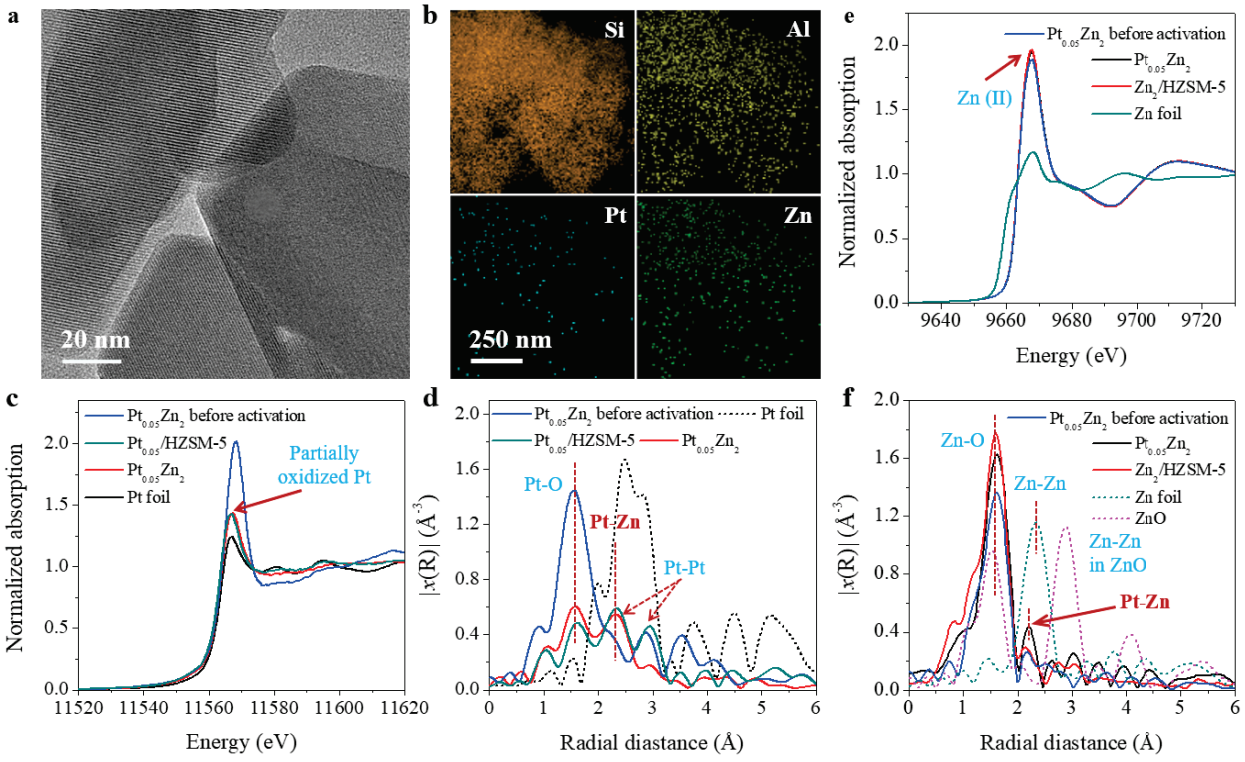

Fig. 3. Characterization of $Pt_{0.05}$-Zn_2/HZSM-5 catalyst. (a-b) HRTEM and STEM-EDS images; (c-d) Pt L_{III}-edge XANES and EXAFS spectra; and (e-f) Zn K-edge XANES and EXAFS spectra.

Structural characterization. The representative electron microscopy images of the $Pt_{0.05}$-Zn_2/HZSM-5 catalyst are shown in Fig. 3 a-b. The absence of nanosized particles from the HRTEM image suggested that larger ZnO and Pt^0 particles were not formed on the external surface of the zeolite. Nonetheless, the STEM-EDS elements mapping demonstrated the homogeneous distribution of Zn and Pt species throughout the zeolite, which is a strong indication of the presence of Zn and Pt species, in proximity, inside the micropore of the HZSM-5 zeolite.

The chemical properties of the Pt and Zn species in the bimetallic $Pt_{0.05}$-Zn_2/HZSM-5 catalyst were further characterized by X-ray absorption spectroscopy. Fig. 3c shows the X-ray absorption near-edge structure (XANES) spectra at Pt L_{III}-edge for the bimetallic $Pt_{0.05}Zn_2$ sample (before and after activation) and the monometallic $Pt_{0.05}$/HZSM-5 and Pt foil references. The white line (see Fig. 3c) of the $Pt_{0.05}Zn_2$ sample before activation is high, indicating that the Pt was in the oxidative form or as $Pt^{\delta+}$ cation exchanged to framework AlO_4^- of the HZSM-5 before activation (in 10% H_2). The white line intensity decreased significantly for both $Pt_{0.05}Zn_2$ and monometallic $Pt_{0.05}$/HZSM-5 after activation, suggesting that the Pt species was being reduced during the activation. Nonetheless, the Pt species are not fully reduced to Pt^0 because the white line intensities are still higher than the Pt foil. The Pt L_{III}-edge k3-weighted Fourier transform of the extended X-ray absorption fine structure (EXAFS) spectra are shown in Fig. 3d. The spectra of the $Pt_{0.05}Zn_2$ sample before activation exhibit a pronounced peak at 1.55 Å originating from the nearest Pt-O scattering corresponding to PtO_2 or single-atom $Pt^{\delta+}$ Lewis acids, which is consistent with the high white line intensity in the XANES spectrum. The Pt-Pt nearest neighbors at R-distance between 2-3 Å, as well as the Pt-Pt next nearest neighbors in Pt oxide at R-distance of 3.5 Å in the $Pt_{0.05}Zn_2$ sample before activation, were small, indicating that the $Pt^{\delta+}$ Lewis acids are the dominant species. After activation, the intensity of the nearest Pt-O scattering decreased, meanwhile a new pronounced peak at 2.33 Å was observed. The peak at 2.33 Å originated from the nearest Pt-Pt scattering for the monometallic $Pt_{0.05}$/HZSM-5 catalyst, while must be assigned to the Pt-Zn coordination for the bimetallic $Pt_{0.05}Zn_2$ sample because the critical peak at 2.95 Å for the Pt-Pt was absent.[43-45] Additionally, the next nearest Pt-Pt scattering in Pt nanoclusters at R-distance above 3 Å is absent, indicating the presence of isolated Pt atoms. Therefore, we suggested that the Pt species in the bimetallic catalysts (after activation) form the "Pt_1-Zn_n" hybrid cluster.

The coordination structures of the Pt species in the monometallic $Pt_{0.05}$/HZSM-5 and bimetallic $Pt_{0.05}$-Zn_2/HZSM-5 catalysts were obtained by fitting the EXAFS spectra. The coordination number (CN), interatomic distance (R), Debye-Waller factor (σ2), and inner potential correction (ΔE) are summarized in Table S2. For the monometallic $Pt_{0.05}$/HZSM-5 catalyst after activation, the CNs of Pt-O and Pt-Pt are 1 and 6, respectively, and the average absorber-back-scatter distance of Pt-O and Pt-Pt are 2 and 2.64 Å, respectively. These results suggested the formation of $[Pt_m\text{-}H_n]^{n+}$ cluster anchored to the framework $Al_fO_4^-$ in the monometallic Pt/HZSM-5 catalyst. For the bimetallic $Pt_{0.05}$-Zn_2/HZSM-5 catalyst, the Pt-Pt coordination was absent and the CNs of Pt-O and Pt-Zn are around 1 and 5, respectively, which again suggested the formation of Pt_1-Zn_n (n=4-6) clusters. The average absorber-back-scatter distance of Pt-Zn is 2.6 Å, which is slightly lower than the Pt-Pt scattering.

The XANES spectra at Zn K-edge are shown in Fig. 3e. From a comparison with Zn foil, the adsorption edge of the bimetallic $Pt_{0.05}Zn_2$ (before and after activation) and monometallic Zn_2/HZSM-5 shifted to higher energy due to the absence of the pre-edge – originated from 1s→3d transition – in the K-edge

since the 3d-subshell in the Zn (II) system is completely filled.[46] Additionally, the bimetallic $Pt_{0.05}Zn_2$ catalysts and Zn_2/HZSM-5 show very similar white line intensity, significantly higher than that for Zn foil, also indicating the presence of Zn (II) rather than Zn^0. The presence of Pt (ultralow loading) and activation in H_2 seem not to affect the overall oxidation state of the Zn species. Noteworthily, our previous in-situ XANES shows that the white line split into two peaks after reduction and reaction,[3, 5] which according to Dokania et al.,[47] might suggest the formation of Zn_6O_6 disordered clusters in the monometallic Zn/HZSM-5 catalyst.

The structure of the Zn (II) species can be further discussed from the Fourier transform of the EXAFS spectra. As shown in Fig. 3f, all the $Pt_{0.05}Zn_2$ and Zn_2/HZSM-5 samples show a pronounced peak at 1.55 Å for the nearest Zn-O scattering, which is consistent with the presence of Zn (II) species according to the XANES. The spectra do not contain a peak at 2.9 Å, which corresponds to the next nearest Zn-Zn neighbors in ZnO, indicating the absence of ZnO crystallites or the presence of ZnO clusters with the substantial disorder.[47] Considering that Zn species was introduced into the zeolite (with a high Si/Al ratio) through ion-exchange, we suggested the formation of isolated Zn (II) cations exchanged to the framework AlO_4^- of the HZSM-5 zeolite rather than the disordered clusters. According to Biscardi et al.,[48] such Zn species are hydrated during the ex-situ experiments and forming …Al-O-Zn(OH) species, which could dehydrate to form "…Al-O-Zn-O-Zn-O-Al…" and "…Al-O-Zn-O-Al…" species during the reaction. Although we can not exclude the formation of single-site or binuclear ZnO_x species anchored to the Si-OH groups as suggested by Zhao et al. with silicalite-1 as the support,[41] such species should not dominate the present catalysts since the concentration of the Si-OH groups in the HZSM-5 is significantly lower than the Brønsted acid Si-OH-Al (vide infra).

By fitting the EXAFS spectra, the CN of Zn-O is identified to be ~6 (see Table S2), which suggested the octahedral structured Zn sites when the catalysts were hydrated. Additionally, the Zn_2/HZSM-5 and $Pt_{0.05}Zn_2$ (before activation) samples do not contain a peak at R-distance of 2.34 Å, corresponding to Zn-Zn nearest neighbors in Zn foil. Nonetheless, for the $Pt_{0.05}Zn_2$ catalyst after activation, a small peak at 2.2 Å – shifted to a low-R compared to that of the Zn foil – can be identified. This small peak must be originated from the Zn-Pt scattering[43-45] as already discussed based on the Pt L_{III}-edge EXAFS spectrum. Therefore, the Pt_1-Zn_n hybrid cluster must be positively charged, namely $[Pt_1\text{-}Zn_n]^{\delta+}$ cluster anchored through the Zn^+-O^- bond inside the HZSM-5.

Acidity and metal/acid proximity. The influence of Zn and Pt species on the acidity of the HZSM-5 zeolite was characterized by in-situ NH_3-DRIFT (diffuse reflectance infrared Fourier transform) spectroscopy in combination with NH_3-TPD (temperature-programmed desorption). The NH_3-DRIFT spectra (with clean surface fresh catalyst as the background) show negative bands at wavenumbers between 3500-3800 cm^{-1} (see Fig. 4a, upper panel) after NH_3 adsorption at 350°C, indicating that the O-H stretching vibrations in the fresh catalyst are disappeared after NH_3 adsorption. Specifically, the band at 3600 cm^{-1} corresponds to the Brønsted acid Si-OH-Al, and the bands at 3655 and 3743 cm^{-1} correspond to the extraframework Al-OH groups and the Si-OH groups at defect sites, respectively.[49] After flushing the NH_3 pre-adsorbed samples with Ar at the same temperature for 20 min, the negative bands at 3655 and 3743 cm^{-1} almost disappeared (Fig. 4a, lower panel), consistent with the NH_3-TPD profiles that NH_3 was desorbed from the weak acid sites at temperatures below 350 °C (see Fig. S8). In

terms of the relative intensity of the band at 3600 cm^{-1}, it is seen that the $Pt_{0.05}$/HZSM-5 and HZSM-5 show almost identical intensity, indicating the presence of Pt (0.05 wt%) does not decrease the Brønsted acid density. Whereas the band intensity significantly decreased for the samples containing Zn, which confirms that the Zn (II) cations were primarily exchanged at the Brønsted acid sites. Noteworthily, the $Pt_{0.01}Zn_2$ sample shows high band intensity than the Zn_2/HZSM-5. Therefore, the presence of Pt, due to the formation of $[Pt_1\text{-}Zn_n]^{\delta+}$ clusters, regenerates part of the Brønsted acids that were originally occupied by the Zn (II) cations through ion-exchange.

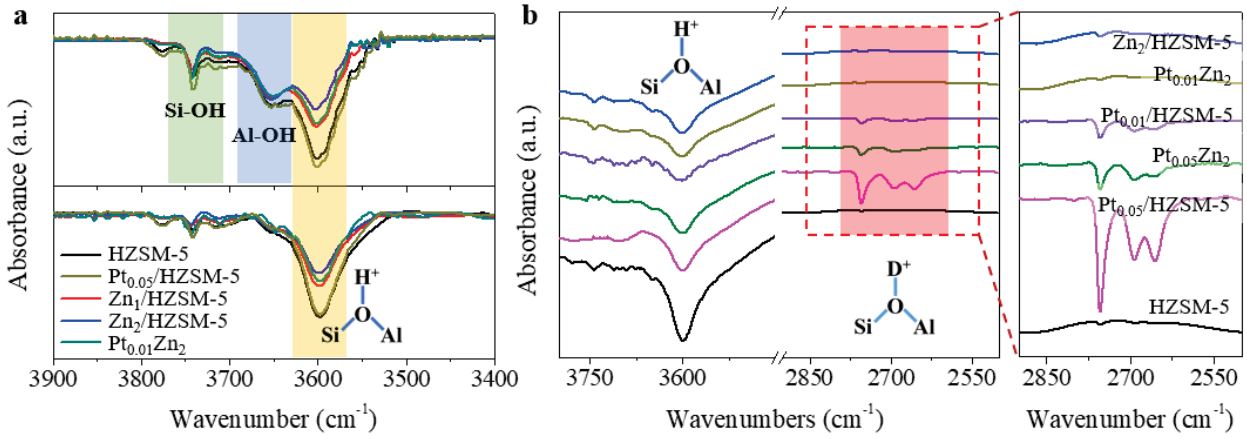

Fig. 4. In-situ DRIFT characterizations. (a) NH_3-DRIFT spectra: under NH_3 for 20 min (upper panel) and after flushing by Ar for 30 min (lower panel); (b) NH_3-DRIFT spectra after H/D isotopic exchange at room temperature in pure D_2 for 10 min. All of the spectra were collected at 350 ºC.

The proximity between the metal and Brønsted acid sites was investigated based on the NH_3-DRIFT spectroscopy of the H/D exchanged (at room temperature, RT) samples. The H/D isotopic exchange between proton (H^+) and D_2 can be realized at RT only when the metal and acid sites are in close proximity, forming $[Pt_m\text{-}H_n]^{n+}$: Pt^0 clusters-proton adducts.[50] The extent of isotopic exchange was characterized by the same NH_3-DRIFT method discussed above. As shown in Fig. 4b, isotopic exchange with D_2 at RT does not change the NH_3-DRIFT spectrum for the HZSM-5. Therefore, it confirms the absence of proton (H^+) and D_2 exchange at RT without the metal sites. Nonetheless, for the monometallic $Pt_{0.05}$/HZSM-5 catalyst, the intensity of the original band for Brønsted acid sites (Si-OH-Al) at 3600 cm^{-1} significantly decreased after the isotopic exchange at RT. Meanwhile, new bands at wavenumber between 2600 and 2800 cm^{-1} were identified. Such bands can be assigned to the Brønsted acid Si-OD-Al vibration possibly at different locations. The intensity of the bands at 2600-2800 cm^{-1} significantly decreased with decreasing Pt loading from 0.05 to 0.01 wt%, suggesting the critical role of the Pt sites on the isotopic exchange. In contrast to the monometallic Pt/HZSM-5, the Zn_2/HZSM-5 catalyst also shows the absence of the proton (H^+) and D_2 exchange at RT, which is not a surprise since the Zn (II) cations are replacing the proton rather than forming metal-proton adduct during ion-exchange. More importantly, the bimetallic $Pt_{0.05}Zn_2$ shows significantly lower band intensity at 2600-2800 cm^{-1} than the monometallic $Pt_{0.05}$/HZSM-5. Therefore, only a small amount of Pt in the bimetallic catalysts forms the Pt^0 clusters-proton adducts; most of the Pt species are forming $[Pt_1\text{-}Zn_n]^{\delta+}$ clusters as aforementioned. Specifically, the $Pt_{0.01}Zn_2$ catalyst shows the absence of the isotopic exchange, indicating the formation of $[Pt_1\text{-}Zn_n]^{\delta+}$ clusters exclusively at ultralow Pt loading (≤0.01 wt%). The isotopic exchange between proton (H^+) and D_2 discussed above is also supported by

the in-situ mass spectrometry (MS). The signals of m/z=3 for HD during the isotopic exchange at RT for different samples are shown in Fig. S9. Consistent with the NH_3-DRIFT results, significant HD formation was only identified for the monometallic $Pt_{0.05}$/HZSM-5 catalyst.

Discussion. Through correlating the catalytic data with the structural/acidity characterizations, we suggested that the formation of $[Pt_1\text{-}Zn_n]^{\delta+}$ clusters, instead of the Pt^0 clusters-proton adducts, be responsible for the outstanding catalytic performance. The Pt^0 cluster has a high affinity for the paraffinic C-H bond, which renders its exceptional activity in catalyzing hydrocarbons dehydrogenation. As shown in Fig. S10, the monometallic $Pt_{0.05}$/HZSM-5 catalysts show very high activity during C_2H_6/D_2 exchange at 300 ºC. The specific activities for the formation of C_2H_5D, $C_2H_4D_2$, and $C_2H_3D_3$ are up to 1044, 310, and 77 μmol/gcat/min, respectively. Nonetheless, the Pt^0 cluster also demonstrates strong interaction with the olefinic intermediates, which might be the key reason for the fast deactivation with the monometallic Pt/HZSM-5 catalysts. The ethylene-TPD (temperature-programmed desorption) profiles for different catalysts are shown in Fig. S11. During ethylene-TPD, ethylene is actually absent from the desorption profiles, instead, various products, including $C_{3\text{-}6}$ olefins, C_{2+} alkanes, and BTX, were desorbed, indicating the strong interaction and fast oligomerization of the ethylene intermediate. We suggested that the rate of catalyst deactivation increases with decreasing Pt loading (see Fig. 2) because the adsorption of olefinic intermediates further increases with decreasing Pt^0 cluster size (increasing the electron deficiency of the Pt^0 clusters). Additionally, the Pt ensembles in the Pt^0 clusters are active for C-C cleavage through cracking/hydrogenolysis, which resulted in the formation of either CH_4 (by-product) or coke deposition after deep dehydrogenation. Consequently, the Pt catalysts during hydrocarbon processing were frequently modified by Cu,[51] Zn,[34] Sn,[52] *etc*. to form either a single atom alloy or intermetallic alloy to optimize the functionalities of the Pt species.

In the bimetallic $Pt_x\text{-}Zn_y$/HZSM-5 catalysts, the Pt species forming $[Pt_1\text{-}Zn_n]^{\delta+}$ cluster with the Zn species. Such a cluster is still quite active for the C-H bond activation according to the C_2H_6/D_2 exchange (see Fig. S10), although the activity is significantly lower than the Pt^0 clusters. Note that the Lewis acid Zn (II) cation is inactive for the C_2H_6/D_2 exchange under the investigated conditions. Therefore, the activity identified for the $[Pt_1\text{-}Zn_n]^{\delta+}$ cluster must originate from the Pt sites. The formation of $[Pt_1\text{-}Zn_n]^{\delta+}$ cluster could change the electronic properties of the Pt species in Pt^0 cluster. For example, the isolated Pt in $(\equiv SiOZn)_{4\text{-}6}$ cluster (in the dealuminated beta zeolite) has been identified as a highly efficient catalyst for light alkanes dehydrogenation by Bell and coworkers.[45, 53] According to Gong and coworkers,[43] isolated Pt in $[PtZn_4]$ ensembles can only contact C_3H_5 through a single bond instead of more stable three Pt-C interactions in $[Pt_3]$ ensembles, which is quietly similar to the present $[Pt_1\text{-}Zn_n]^{\delta+}$ cluster. Additionally, the electron-rich Pt in the $[Pt_1\text{-}Zn_n]^{\delta+}$ cluster (in contrast to Pt^0 clusters-proton adducts) further promotes the desorption of olefinic intermediates. It is seen from the ethylene-TPD profiles that the bimetallic $Pt_{0.01}Zn_2$/HZSM-5 catalyst shows very similar desorption behavior to the Zn_2/HZSM-5, but the peak temperature of BTX decreased. In contrast to the HZSM-5 and $Pt_{0.01}$/HZSM-5, desorption of olefins at low temperatures (~200°C) was enhanced. Therefore, the bimetallic catalysts demonstrated outstanding stability in ethane DHA. The rate of catalyst deactivation for the bimetallic catalysts decreases with decreasing Pt loading (see Fig. 2) because the Pt species form $[Pt_1\text{-}Zn_n]^{\delta+}$ clusters exclusively at ultralow Pt loading (≤0.01 wt%). At a higher Pt loading, a

portion of the Pt species could still form Pt^0 cluster-proton adducts with the excess Brønsted acid sites, which is responsible for the slightly enhanced rate of deactivation.

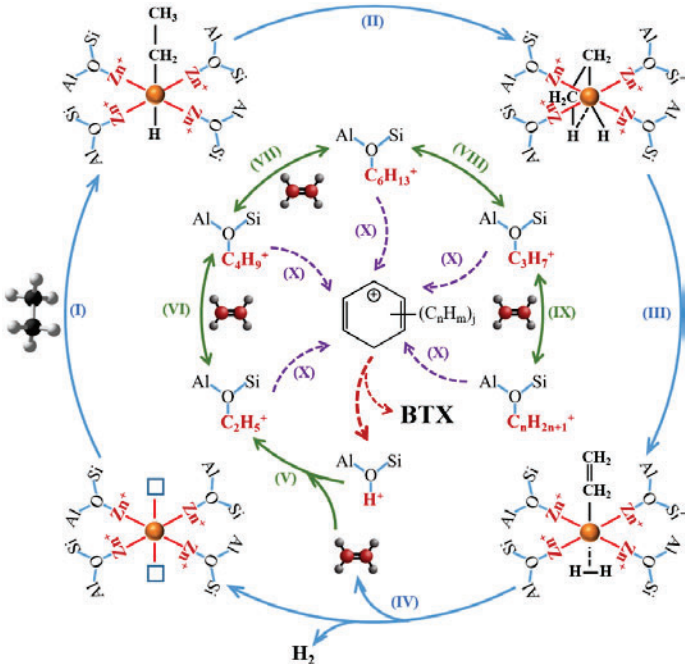

Fig. 5. Proposed bifunctional reaction mechanism for ethane DHA on the $[Pt_1\text{-}Zn_n]^{\delta+}$ and Brønsted acid sites.

Turning to the catalytic mechanism, we propose that aromatics were produced through the bifunctional pathways, involving dehydrogenation over the $[Pt_1\text{-}Zn_n]^{\delta+}$ clusters, oligomerization/cyclization over the Brønsted acid sites, and dehydrogenation or hydride transfer over both metal and acid sites (see Fig. 5). According to Bell and coworkers,[45] we suggest that the DHA reaction was initiated with ethane dissociative adsorption on the $[Pt_1\text{-}Zn_n]^{\delta+}$ (step I) leads to an ethyl group and an H atom bonded to the Pt atom. Then the second hydrogen dissociation took place on the same Pt atom (steps II and III), which followed the desorption of ethylene and H_2 (step IV). Ethylene desorbed from the Pt atom can be easily re-adsorbed on the Brønsted acid site – protonated with H^+ – forming $C_2H_5^+ \cdot AlO_4^-$ carbocation species (step V), which was followed by oligomerization/cracking to form higher olefins (steps VI-IX). In-situ ethylene-TPD-DRIFT analysis (see Fig. S12) suggested the formation of $C_nH_{2n+1}^+ \cdot AlO_4^-$ when exposing the catalyst to ethylene at 100 ºC, which was evidenced by the presence of IR bands at 2800-3000 cm^{-1}, corresponding to the C-H stretching of CH_2 and CH_3. These bands gradually decreased with increasing temperature above 250 ºC and almost disappeared above 450 ºC. The mixed olefins, subsequently, involve trans-alkylation, dealkylation, isomerization, cyclization, dehydrogenation, hydride transfer, etc., forming a "hydrocarbon pool" inside the zeolite (step X).[19, 54] The composition of the "hydrocarbon pool" was analyzed by GC-MS (see Fig. S13) with a sample obtained by CH_2Cl_2 extraction of the used $Pt_{0.01}\text{-}Zn_2$/HZSM-5 (dissolved in HF). The hydrocarbons confined in the catalyst are mainly composed of higher n-/iso-/cyclo-alkanes and alkenes and alkyl aromatics. Therefore, we suggest that the "hydrocarbon pool" mechanism could be involved after ethane dehydrogenation to ethylene on the $[Pt_1\text{-}Zn_n]^{\delta+}$ clusters. While the conventional "hydrocarbon

pool" mechanism involves the gas phase reaction, the presence of metal sites (Lewis acid Zn (II) cation and $[Pt_1\text{-}Zn_n]^{\delta+}$ clusters) could favor dehydrogenation rather than hydride transfer. The relatively low selectivity of C_{3+} alkanes (see Fig. S4) is strong evidence for this conclusion.

Conclusions

We show that isolated Pt atoms in the $[Pt_1\text{-}Zn_n]^{\delta+}$ clusters@HZSM-5 – single Pt anchored to the Zn (II) cations exchanged to the framework $Al_fO_4^-$ tetrahedral of the ZSM-5 zeolite – are highly efficient for the DHA of ethane (and other light alkanes: results are not shown). Such bimetallic $Pt_x\text{-}Zn_y$/HZSM-5 catalysts contain ultralow Pt loading (0.001-0.05 wt%), whereas show unprecedented high activity and stability. The specific activity of BTX is up to 8.2 mol/g_{Pt}/min (or 1592 min^{-1}) over the $Pt_{0.001}\text{-}Zn_2$/HZSM-5 catalyst during ethane DHA at 550ºC and the rate of catalyst deactivation are up to 120 times lower than the monometallic Pt/HZSM-5 catalysts depend on the Pt loading. We demonstrated that the monometallic Pt/HZSM-5 catalysts are unstable for the DHA reaction due to the formation of Pt^0 cluster-proton adducts. Such species have strong interaction with olefinic intermediates owing to the electron deficiency of the Pt ensembles, therefore the active sites deactivate quickly due to coke deposition. Unlike the Pt^0 clusters, the $[Pt_1\text{-}Zn_n]^{\delta+}$ clusters eliminate the Pt ensembles and behavior similar to the Zn (II) cations during the ethylene-TPD. Therefore, the bimetallic $Pt_x\text{-}Zn_y$/HZSM-5 catalysts show significantly enhanced stability (similar to the Zn_2/HZSM-5) during the DHA. Over the $Pt_{0.01}\text{-}Zn_2$/HZSM-5 catalyst, the formation of BTX remains > 50% of the initial activity after 17 h TOS, and it takes > 65 h for the total deactivation. We anticipate that the concept of fabricating bimetallic clusters (with isolated noble metals) in the zeolites can be extended to other catalytic systems.

Experimental section

Catalyst preparation. Monometallic Zn/HZSM-5 catalysts were synthesized through ion exchange (IE). Typically, 10 g of NH_4-ZSM-5 zeolite (purchased from VWR International with SiO_2/Al_2O_3 = 30 and surface area 400 m^2/g) was exchanged with 200 mL of 0.05 M zinc nitrate aqueous solution at 80 °C under stirring. The Zn_2/HZSM-5 catalyst (Zn loading according to ICP is around 2 wt%) was obtained through IE for 3 days, and the Zn_1/HZSM-5 catalyst (Zn loading around 1 wt%) was obtained through IE for 10 min. The sample was centrifuged and washed with DI water three times then dried at 120 °C for 12 h and calcined in a tube furnace under flowing of air at 550 °C (ramp 5 °C/min) for 6 h.

Bimetallic Pt-Zn/HZSM-5 catalysts were prepared through wet impregnation with the as-prepared Zn/HZSM-5 samples. Specifically, 1 g of Zn/HZSM-5 powder was impregnated with 10 mL of $Pt(NH_3)_4(NO_3)_2$ aqueous solution. The concentration of the solution was adjusted to obtain Pt nominal loading of 0.001, 0.005, 0.01, and 0.05 wt%, respectively. The impregnation was performed at room temperature for 2 h before being transferred to a rotary evaporator to remove water at 65 °C under 150 mbar. The obtained sample was dried at 120 °C for 12 h and calcined in a tube furnace under flowing of dry air at 550 °C (ramp 5 °C/min) for 6 h.

Monometallic Pt/HZSM-5 catalysts were prepared according to the same procedures as described for the bimetallic catalysts except using HZSM-5 instead of Zn/HZSM-5. The HZSM-5 was obtained through the calcination of NH_4-ZSM-5 at 560 °C for 6 h in a muffle furnace.

Catalytic testing. The catalytic performance of ethane DHA was evaluated in the Micromeritics Autochem 2910 setup. For each test, 0.1 g catalyst (25-40 mesh) was mixed with 0.4 g silica sand (pretreated with 70% HNO_3 overnight and calcined at 650 ºC for 5 h) and then loaded into the U-shape quartz reactor. Before catalytic testing, the catalyst was pretreated in 10% H_2/Ar (20 ml/min) at 650ºC (ramp: 10 ºC/min) for 20 min. Before catalytic testing, the spectra of pure Ar and C_2H_6 were collected for the MS calibration. The reaction was performed at 550 ºC and atmospheric pressure with 20 mL/min of pure ethane (gas hourly space velocity (GHSV) 6000 h^{-1}). The reactor effluent was measured by the online Agilent 5973 MS (equipped with MS Sensor 2.0 software, Diablo Analytical, Inc.). The detailed method of MS quantification can be found in our previous paper.[5]

Catalyst characterization. The X-ray absorption spectroscopy in terms of X-ray absorption near edge structure (XANES) and extended X-ray absorption fine structure (EXAFS) measurements were recorded at beamline 12-BM in Advanced Photon Source at Argonne National Laboratory. Data were acquired in fluorescence mode using a 13-element germanium detector set at 90º angle from the incoming beam; the sample was set at a 45º angle to the incoming beam and detector. The samples were pressed to a disk and sealed in Kapton® tape then attached to the sample stage. Spectra were recorded at Pt L_{III} and Zn K edges. The XAS data were normalized and analyzed by Athena software.

Transmission electron microscopy (TEM) images and STEM-EDS chemical mapping were obtained using JEOL 2100TEM (accelerating voltage of 200 kV) equipped with a Gatan camera.

In situ Diffuse Reflectance Infrared Fourier Transform spectroscopy with NH_3 as probe molecule (NH_3-DRIFT) was performed on a Thermo Scientific Nicolet i20 FTIR spectrometer equipped with a liquid-nitrogen cooled Mercury-Cadmium-Telluride (MCT) detector and Praying Mantis™ high-temperature operando reaction chamber (Harrick Scientific Products Inc.) with CaF_2 windows. The spectra were recorded at a resolution of 4 cm^{-1} with accumulations of 32 scans/min. An appropriate amount of the pre-activated powder sample was loaded into the reaction cell, the sample was further activated in-situ at 600 ºC under 20 ml/min of 5% H_2/N_2 for 1 h. Then the temperature of the cell was decreased to 350 ºC and the cell influent was switched to Ar to collect the background spectrum. After that, the reaction cell inlet was switched from Ar to NH_3 at the same temperature and the spectra were recorded after 20 min. Finally, the reaction cell inlet was switched back from NH_3 to Ar, and the spectra were recorded after 30 min. For the In-situ proton (H^+) and D_2 exchange/DRIFT, the sample after activation was decreased to room temperature (30 ºC) for the isotopic exchange. The reaction cell inlet was first switched from 5% H_2/N_2 to Ar and purged for 1 h, then switched to pure D_2 (10 ml/min) and kept for 20 min for isotopic exchange. Then the cell inlet was switched back to Ar and the temperature of the cell was increased to 350 ºC. Finally, the NH_3-DRIFT spectra were recorded according to the same procedures as aforementioned.

ASSOCIATED CONTENT

Supporting Information

Additional catalytic data, EXAFS fitting data, NH_3-TPD, In-situ proton (H^+)/D_2 isotopic exchange, ethane/D_2 isotopic exchange, and ethylene-TPD. This material is available free of charge via the Internet at http://pubs.acs.org.

AUTHOR INFORMATION

Corresponding Author

* yzxiang@che.msstate.edu

Notes

The authors declare no conflict of interest.

Acknowledgments

This research used resources of the Advanced Photon Source, a U.S. Department of Energy (DOE) Office of Science User Facility operated for the DOE Office of Science by Argonne National Laboratory under Contract No. AC02-06CH11357. We acknowledge Daniela Sanchez Arana (Department of Chemistry at Mississippi State University) for her assistance with ICP-MS and GC-MS analysis.

REFERENCE

1. Gomez, E.; Nie, X.; Lee, J. H.; Xie, Z.; Chen, J. G., Tandem Reactions of CO_2 Reduction and Ethane Aromatization. *J. Am. Chem. Soc.* **2019,** *141* (44), 17771-17782.
2. Goodarzi, F.; Thumbayil, R. P.; Enemark-Rasmussen, K.; Mielby, J.; Nguyen, T. T. M.; Beato, P.; Joensen, F.; Kegnæs, S., Enhanced Catalytic Performance of Zn-containing HZSM-5 upon Selective Desilication in Ethane Dehydroaromatization Process. *ChemCatChem* **2020,** *12* (5), 1519-1526.
3. Liang, T.; Toghiani, H.; Xiang, Y., Transient Kinetic Study of Ethane and Ethylene Aromatization over Zinc-Exchanged HZSM-5 Catalyst. *Ind. Eng. Chem. Res.* **2018,** *57* (45), 15301-15309.
4. Xiang, Y.; Wang, H.; Cheng, J.; Matsubu, J., Progress and prospects in catalytic ethane aromatization. *Catal. Sci. Technol.* **2018,** *8* (6), 1500-1516.
5. Liang, T.; Fadaeerayeni, S.; Shan, J.; Li, T.; Wang, H.; Cheng, J.; Toghiani, H.; Xiang, Y., Ethane Aromatization over Zn-HZSM-5: Early-Stage Acidity/Performance Relationships and Deactivation Kinetics. *Ind. Eng. Chem. Res.* **2019,** *58* (38), 17699-17708.
6. Fadaeerayeni, S.; Shan, J.; Sarnello, E.; Xu, H.; Wang, H.; Cheng, J.; Li, T.; Toghiani, H.; Xiang, Y., Nickel/gallium modified HZSM-5 for ethane aromatization: Influence of metal function on reactivity and stability. *Appl. Catal. A* **2020,** *601*, 117629.
7. Razdan, N. K.; Bhan, A., Carbidic Mo is the sole kinetically-relevant active site for catalytic methane dehydroaromatization on Mo/H-ZSM-5. *J. Catal.* **2020,** *389*, 667-676.
8. Uslamin, E. A.; Saito, H.; Sekine, Y.; Hensen, E. J. M.; Kosinov, N., Different mechanisms of ethane aromatization over Mo/ZSM-5 and Ga/ZSM-5 catalysts. *Catal. Today* **2021,** *369*, 184-192.
9. Zhou, W.; Liu, J.; Wang, J.; Lin, L.; Zhang, X.; He, N.; Liu, C.; Guo, H., Enhancing Propane Aromatization Performance of Zn/H-ZSM-5 Zeolite Catalyst with Pt Promotion: Effect of the Third Metal Additive-Sn. *Catal. Lett.* **2019,** *149* (8), 2064-2077.
10. Xu, B.; Tan, M.; Wu, X.; Geng, H.; Song, F.; Ma, Q.; Luan, C.; Yang, G.; Tan, Y., Effects of silylation on Ga/HZSM-5 for improved propane dehydroaromatization. *Fuel* **2021,** *283*, 118889.
11. Arzumanov, S. S.; Gabrienko, A. A.; Toktarev, A. V.; Lashchinskaya, Z. N.; Freude, D.; Haase, J.; Stepanov, A. G., Propane Transformation on Zn-Modified Zeolite. Effect of the Nature of Zn Species on Alkane Aromatization and Hydrogenolysis. *J. Phys. Chem. C* **2019,** *123* (50), 30473-30485.

12.https://www.eia.gov/dnav/pet/hist/LeafHandler.ashx?n=PET&s=M_EPL2_FPF_NUS_MBBLD&f=M. date of access: June 10, 2022
13. Cox, H. UOP CYCLAR PROCESS. In *Handbook of Petroleum Refining Processes*, 4th ed.; Meyers, R. A., Ed. McGraw-Hill Education: New York, 2016; pp 65-71.
14. Fadaeerayeni, S.; Chen, G.; Toghiani, H.; Xiang, Y., Mechanism and Kinetics of Ethane Aromatization According to the Chemical Transient Analysis. *Top. Catal.* **2020,** *63* (15-18), 1463-1473.
15. Hagen, A.; Roessner, F., Ethane to Aromatic Hydrocarbons: Past, Present, Future. *Catal. Rev.: Sci. Eng.* **2000,** *42* (4), 403-437.
16. Dufresne, L. A.; Le Van Mao, R., Hydrogen back-spillover effects in the aromatization of ethylene on hybrid ZSM-5 catalysts. *Catal. Lett.* **1994,** *25* (3), 371-383.
17. Le van Mao, R.; Yao, J.; Dufresne, L. A.; Carli, R., Hybrid catalysts containing zeolite ZSM-5 and supported gallium oxide in the aromatization of n-butane. *Catal. Today* **1996,** *31* (3), 247-255.
18. Le Van Mao, R.; Dufresne, L.; Yao, J., Long distance hydrogen back-spillover (LD-HBS) phenomena in the aromatization of light alkanes. *Appl. Catal.* **1990,** *65* (1), 143-157.
19. Chen, G.; Liu, H.; Fadaeerayeni, S.; Shan, J.; Xing, A.; Cheng, J.; Wang, H.; Xiang, Y., Tuning the reactivity of ethylene oligomerization by HZSM-5 framework Al_f proximity. *Catal. Sci. Technol.* **2020,** *10* (12), 4019-4029.
20. Bragin, O. V.; Shpiro, E. S.; Preobrazhensky, A. V.; Isaev, S. A.; Vasina, T. V.; Dyusenbina, B. B.; Antoshin, G. V.; Minachev, K. M., The state of platinum in high-silica zeolites and its catalytic activity in ethane and propane aromatization. *Appl. Catal.* **1986,** *27* (2), 219-231.
21. Steinberg, K.-H.; Mroczek, U.; Roessner, F., Aromatization of ethane on platinum containing ZSM-5 zeolites. *Appl. Catal.* **1990,** *66* (1), 37-44.
22. Vosmerikova, L. N.; Barbashin, Y. E.; Vosmerikov, A. V., Catalytic aromatization of ethane on zinc-modified zeolites of various framework types. *Pet. Chem.* **2014,** *54* (6), 420-425.
23. Mehdad, A.; Lobo, R. F., Ethane and ethylene aromatization on zinc-containing zeolites. *Catal. Sci. Technol.* **2017,** *7* (16), 3562-3572.
24. Choudhary, V. R.; Kinage, A. K.; Choudhary, T. V., Effective Low-Temperature Aromatization of Ethane over H-Galloaluminosilicate(MFI) Zeolites in the Presence of Higher Alkanes or Olefins. *Angew. Chem. Int. Ed.* **1997,** *36* (12), 1305-1308.
25. Samanta, A.; Bai, X.; Robinson, B.; Chen, H.; Hu, J., Conversion of Light Alkane to Value-Added Chemicals over ZSM-5/Metal Promoted Catalysts. *Ind. Eng. Chem. Res.* **2017,** *56* (39), 11006-11012.
26. Anunziata, O. A.; Eimer, G. A.; Pierella, L. B., Ethane conversion into aromatic hydrocarbons over molybdenum-containing MEL zeolites. *Appl. Catal. A* **1999,** *182* (2), 267-274.
27. Ye, J.; Bai, L.; Liu, B.; Tian, H.; Hu, J.; Polo-Garzon, F.; Mayes, R. T.; Wu, Z.; Fang, Y., Fabrication of a Pillared ZSM-5 Framework for Shape Selectivity of Ethane Dehydroaromatization. *Ind. Eng. Chem. Res.* **2019,** *58* (17), 7094-7106.
28. Iyer, M. V.; Lauritzen, A. M.; Madgavkar, A. M. Process for the conversion of mixed lower alkanes to aromatic hydrocarbons. **2014**, US8835706B2.
29. Lauritzen, A. M.; Madgavkar, A. M., Process for the conversion of lower alkanes to aromatic hydrocarbons. Google Patents. **2014**, US8809608
30. Lauritzen, A. M.; Madgavkar, A. M., Process for the conversion of ethane to aromatic hydrocarbons. **2015**, US9144790
31. Wang;, H.; Xiang;, Y.; Matsubu;, J.; Shan;, J.; Cheng;, J.; Sun;, Q.; Nguyen, L. Method for aromatization of light alkanes. **2020**, US20200207683A1
32. Mitchell, S. F.; Juttu, G. G.; Smith, R. S., Process for alkane aromatization using platinum-zeolite catalyst. **2007**, US7186871

33. Sattler, J. J. H. B.; Ruiz-Martinez, J.; Santillan-Jimenez, E.; Weckhuysen, B. M., Catalytic Dehydrogenation of Light Alkanes on Metals and Metal Oxides. *Chem. Rev.* **2014,** *114* (20), 10613-10653.
34. Cybulskis, V. J.; Bukowski, B. C.; Tseng, H.-T.; Gallagher, J. R.; Wu, Z.; Wegener, E.; Kropf, A. J.; Ravel, B.; Ribeiro, F. H.; Greeley, J.; Miller, J. T., Zinc Promotion of Platinum for Catalytic Light Alkane Dehydrogenation: Insights into Geometric and Electronic Effects. *ACS Catal.* **2017,** *7* (6), 4173-4181.
35. Lapidus, A. L.; Dergachev, A. A.; Kostina, V. A.; Silakova, A. A., Ethane aromatization on Ga-Pt pentasil zeolites. *Pet. Chem.* **2008,** *48* (2), 83-86.
36. Goodarzi, F.; Christensen, D. B.; Joensen, F.; Kegnæs, S.; Mielby, J., The effect of active site distribution in bi-functional Pt-zeolite catalysts for ethane dehydroaromatization. *Appl. Catal. A* **2020,** *592*, 117383.
37. Reschetilowski, W.; Mroczek, U.; Steinberg, K. H.; Wendlandt, K. P., Influence of platinum dispersion on the ethane aromatization on Pt/H-ZSM-5 zeolites. *Appl. Catal.* **1991,** *78* (2), 257-264.
38. Hammer, B.; Nørskov, J. K., Electronic factors determining the reactivity of metal surfaces. *Surf. Sci.* **1995,** *343* (3), 211-220.
39. Levenspiel, O., Experimental search for a simple rate equation to describe deactivating porous catalyst particles. *J. Catal.* **1972,** *25* (2), 265-272.
40. Fuentes, G. A., Catalyst deactivation and steady-state activity: A generalized power-law equation model. *Appl. Catal.* **1985,** *15* (1), 33-40.
41. Zhao, D.; Tian, X.; Doronkin, D. E.; Han, S.; Kondratenko, V. A.; Grunwaldt, J. D.; Perechodjuk, A.; Vuong, T. H.; Rabeah, J.; Eckelt, R.; Rodemerck, U.; Linke, D.; Jiang, G.; Jiao, H.; Kondratenko, E. V., In situ formation of ZnO_x species for efficient propane dehydrogenation. *Nature* **2021,** *599* (7884), 234-238.
42. Moliner, M.; Gabay, J. E.; Kliewer, C. E.; Carr, R. T.; Guzman, J.; Casty, G. L.; Serna, P.; Corma, A., Reversible Transformation of Pt Nanoparticles into Single Atoms inside High-Silica Chabazite Zeolite. *J. Am. Chem. Soc.* **2016,** *138* (48), 15743-15750.
43. Chen, S.; Zhao, Z.-J.; Mu, R.; Chang, X.; Luo, J.; Purdy, S. C.; Kropf, A. J.; Sun, G.; Pei, C.; Miller, J. T.; Zhou, X.; Vovk, E.; Yang, Y.; Gong, J., Propane Dehydrogenation on Single-Site [$PtZn_4$] Intermetallic Catalysts. *Chem* **2021,** *7* (2), 387-405.
44. Sun, Q.; Wang, N.; Fan, Q.; Zeng, L.; Mayoral, A.; Miao, S.; Yang, R.; Jiang, Z.; Zhou, W.; Zhang, J.; Zhang, T.; Xu, J.; Zhang, P.; Cheng, J.; Yang, D.-C.; Jia, R.; Li, L.; Zhang, Q.; Wang, Y.; Terasaki, O.; Yu, J., Subnanometer Bimetallic Platinum–Zinc Clusters in Zeolites for Propane Dehydrogenation. *Angew. Chem. Int. Ed.* **2020,** *59* (44), 19450-19459.
45. Qi, L.; Babucci, M.; Zhang, Y.; Lund, A.; Liu, L.; Li, J.; Chen, Y.; Hoffman, A. S.; Bare, S. R.; Han, Y.; Gates, B. C.; Bell, A. T., Propane Dehydrogenation Catalyzed by Isolated Pt Atoms in identical with ≡SiOZn-OH Nests in Dealuminated Zeolite Beta. *J. Am. Chem. Soc.* **2021,** *143* (50), 21364-21378.
46. Qi, G.; Xu, J.; Su, J.; Chen, J.; Wang, X.; Deng, F., Low-Temperature Reactivity of Zn^+ Ions Confined in ZSM-5 Zeolite toward Carbon Monoxide Oxidation: Insight from in Situ DRIFT and ESR Spectroscopy. *J. Am. Chem. Soc.* **2013,** *135* (18), 6762-6765.
47. Dokania, A.; Ould-Chikh, S.; Ramirez, A.; Cerrillo, J. L.; Aguilar, A.; Russkikh, A.; Alkhalaf, A.; Hita, I.; Bavykina, A.; Shterk, G.; Wehbe, N.; Prat, A.; Lahera, E.; Castaño, P.; Fonda, E.; Hazemann, J.-L.; Gascon, J., Designing a Multifunctional Catalyst for the Direct Production of Gasoline-Range Isoparaffins from CO_2. *JACS Au* **2021,** *1* (11), 1961-1974.
48. Biscardi, J. A.; Meitzner, G. D.; Iglesia, E., Structure and Density of Active Zn Species in Zn/H-ZSM5 Propane Aromatization Catalysts. *J. Catal.* **1998,** *179* (1), 192-202.
49. Nozik, D.; Tinga, F. M. P.; Bell, A. T., Propane Dehydrogenation and Cracking over Zn/H-MFI Prepared by Solid-State Ion Exchange of $ZnCl_2$. *ACS Catal.* **2021**, 14489-14506.
50. Xu, L.; Zhang, Z.; Marshik, B.; Sachtler, W. M. H., Hydrogen isotope exchange on Pd/NaY and Pd/HY zeolites. *Catal. Lett.* **1991,** *10* (1), 121-129.

51. Marcinkowski, M. D.; Darby, M. T.; Liu, J.; Wimble, J. M.; Lucci, F. R.; Lee, S.; Michaelides, A.; Flytzani-Stephanopoulos, M.; Stamatakis, M.; Sykes, E. C. H., Pt/Cu single-atom alloys as coke-resistant catalysts for efficient C-H activation. *Nat. Chem.* **2018,** *10* (3), 325-332.
52. Motagamwala, A. H.; Almallahi, R.; Wortman, J.; Igenegbai, V. O.; Linic, S., Stable and selective catalysts for propane dehydrogenation operating at thermodynamic limit. *Science* **2021,** *373* (6551), 217-222.
53. Zhang, Y.; Qi, L.; Leonhardt, B.; Bell, A. T., Mechanism and Kinetics of n-Butane Dehydrogenation to 1,3-Butadiene Catalyzed by Isolated Pt Sites Grafted onto ≡SiOZn–OH Nests in Dealuminated Zeolite Beta. *ACS Catal.* **2022**, *12*, 3333-3345.
54. Uslamin, E. A.; Saito, H.; Kosinov, N.; Pidko, E.; Sekine, Y.; Hensen, E. J. M., Aromatization of ethylene over zeolite-based catalysts. *Catal. Sci. Technol.* **2020,** *10* (9), 2774-2785.

TOC

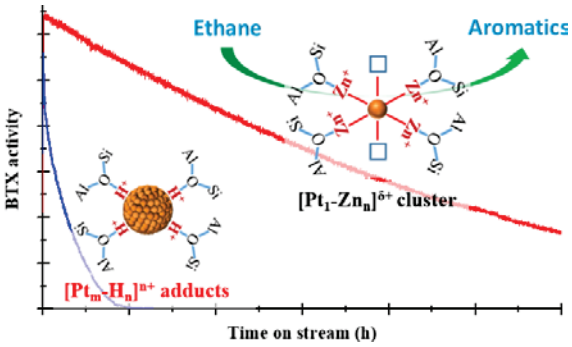
Ethane
Aromatics
BTX activity
Time on stream (h)
[Pt1-Znn]δ+ cluster
[Ptm-Hn]n+ adducts